Cell

Interaction of Circadian Clock Proteins CRY1 and PER2 Is Modulated by Zinc Binding and Disulfide Bond Formation

Ira Schmalen,[1] Silke Reischl,[3] Thomas Wallach,[3] Roman Klemz,[3] Astrid Grudziecki,[3] J. Rajan Prabu,[1] Christian Benda,[1] Achim Kramer,[3,*] and Eva Wolf[1,2,4,*]

[1]Department of Structural Cell Biology, Max Planck Institute of Biochemistry, Am Klopferspitz 18, 82152 Martinsried/Munich, Germany

[2]Department of Physiological Chemistry, Butenandt Institute, Ludwig Maximilians University of Munich, Butenandtstrasse 5, 81377 Munich, Germany

[3]Laboratory of Chronobiology, Charité Universitätsmedizin Berlin, Hessische Strasse 3-4, 10115 Berlin, Germany

[4]Present address: Institut für Allgemeine Botanik, Johannes Gutenberg-University Mainz, Johannes-von-Müllerweg 6 and Institute of Molecular Biology (IMB), 55128 Mainz, Germany

*Correspondence: achim.kramer@charite.de (A.K.), evawolf1@uni-mainz.de (E.W.)

http://dx.doi.org/10.1016/j.cell.2014.03.057

SUMMARY

Period (PER) proteins are essential components of the mammalian circadian clock. They form complexes with cryptochromes (CRY), which negatively regulate CLOCK/BMAL1-dependent transactivation of clock and clock-controlled genes. To define the roles of mammalian CRY/PER complexes in the circadian clock, we have determined the crystal structure of a complex comprising the photolyase homology region of mouse CRY1 (mCRY1) and a C-terminal mouse PER2 (mPER2) fragment. mPER2 winds around the helical mCRY1 domain covering the binding sites of FBXL3 and CLOCK/BMAL1, but not the FAD binding pocket. Our structure revealed an unexpected zinc ion in one interface, which stabilizes mCRY1-mPER2 interactions in vivo. We provide evidence that mCRY1/mPER2 complex formation is modulated by an interplay of zinc binding and mCRY1 disulfide bond formation, which may be influenced by the redox state of the cell. Our studies may allow for the development of circadian and metabolic modulators.

INTRODUCTION

In mammals, many physiological, metabolic, and behavioral processes are regulated in a daytime-dependent manner. Circadian (~24 hr) rhythms are generated by endogenous circadian clocks, which are operated by interconnected transcriptional and translational feedback loops (Young and Kay, 2001). Additionally, the cellular redox state plays an essential role in circadian clock regulation and links the clock to the cell's metabolic state (Eckel-Mahan and Sassone-Corsi, 2009). In anucleate human red blood cells, several circadian oxidation rhythms have been described, including cysteine oxidation cycles in the H_2O_2 scavenging peroxiredoxins, the daily rhythmic transition between dimeric (mostly oxidized) and tetrameric (mostly reduced) hemoglobin, and daily nicotinamide adenine dinucleotide (NADH)/nicotinamide adenine dinucleotide phosphate (NADPH) oscillations (O'Neill and Reddy, 2011). Furthermore, circadian cycles of peroxiredoxin oxidation occur in all kingdoms of life and are interconnected with the circadian gene-regulatory transcriptional feedback loops in DNA-containing cells (Edgar et al., 2012; O'Neill and Reddy, 2011; O'Neill et al., 2011).

In the canonical gene-regulatory feedback loop of the mammalian circadian clock, the basic helix-loop-helix (bHLH)-PAS (PER-ARNT-SIM) transcription factors BMAL1 and CLOCK activate the transcription of three period (*Per1*, *2*, and *3*) and two cryptochrome (*Cry1* and *2*) clock genes. CRY proteins repress the transcriptional activity of the CLOCK/BMAL1 complex toward the *Cry* and *Per* genes (Griffin et al., 1999; Kume et al., 1999; van der Horst et al., 1999), as well as a large number of clock-controlled genes regulating circadian physiology (Koike et al., 2012). Additionally, CRYs are involved in the regulation of glucose homeostasis, insulin secretion, and tissue-specific insulin sensitivity (Barclay et al., 2013; Lamia et al., 2011; Zhang et al., 2010).

The CRY repressor activity is determined by posttranslational modifications, as well as the daily rhythmic synthesis, nuclear translocation, and degradation of CRYs, which are controlled by interactions with PER1/2 (Yagita et al., 2002) and with the E3 ligase components FBXL3 (Gatfield and Schibler, 2007) and FBXL21 (Hirano et al., 2013; Yoo et al., 2013). The CRY tails and the most C-terminal helix (α22) of the cryptochrome photolyase homology region (PHR) (Figure 1A) are involved in transcriptional repression of CLOCK/BMAL1 (Chaves et al., 2006) and BMAL1 binding (Czarna et al., 2011). The PHR interacts with C-terminal regions of PER1 and PER2 (Eide et al., 2002; Miyazaki et al., 2001; Ozber et al., 2010; Tomita et al., 2010; Yagita et al., 2002), with FBXL3 (Lamia et al., 2009; Xing et al., 2013), FBXL21 (Hirano et al., 2013; Yoo et al., 2013) and with the PAS domains of CLOCK (Huang et al., 2012).

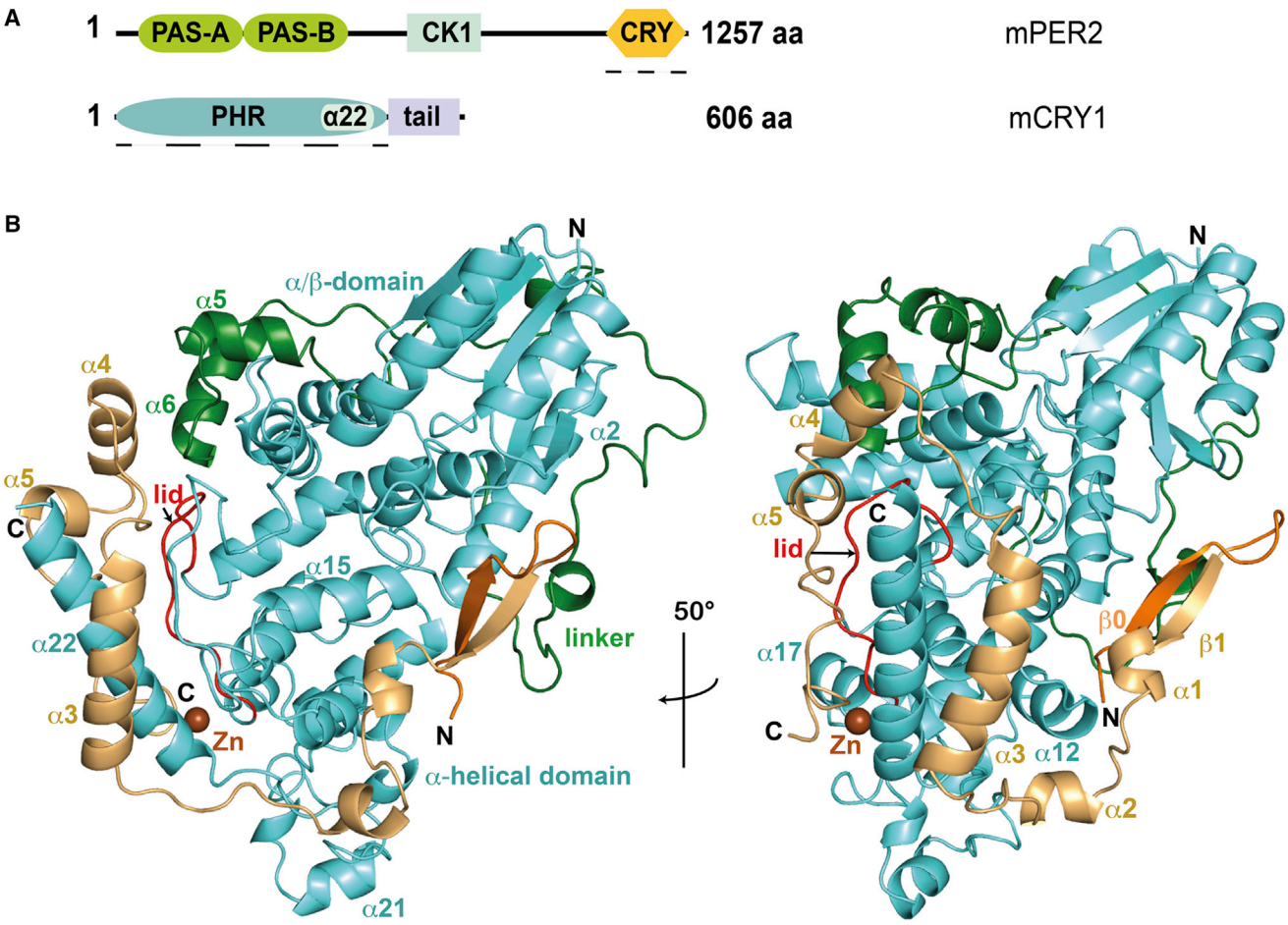

Figure 1. Domain Architecture and Crystal Structure of mCRY1/mPER2 Heterodimer

(A) Domain architecture of mouse CRY1 and PER2. Two PAS domains (PAS-A and PAS-B) and the CK1ε/δ- and CRY-binding regions of mPER2 are shown. mCRY1 comprises a PHR, including helix α22 and a nonconserved C-terminal tail. Dashed lines indicate crystallized fragments.

(B) Ribbon presentation of mCRY1[1–496] (PHR; cyan) in complex with mPER2[1132–1252] (yellow). Green, linker connecting the α/β- and α-helical domain of the mCRY1-PHR. Brown, zinc ion at the mCRY1-mPER2 interface. Red line, C-terminal lid of mCRY1.

See also Figures S1 and S2 and Table S1.

Phosphorylation of Ser71 by AMP kinase (AMPK) in response to the cell's metabolic state reduces CRY1 stability by enhancing FBXL3 binding and weakening PER2 binding (Lamia et al., 2009). Furthermore, PER2 is reported to compete for CRY1 binding to the CLOCK/BMAL1-E-box complex (Ye et al., 2011). These data suggest that PER2 might have overlapping CRY1-binding sites with FBXL3 and CLOCK/BMAL1, which play a role in the regulation of CRY1 stability and transcriptional repression activity. Indeed, our mouse CRY1 (mCRY1) crystal structure revealed partly overlapping mCRY1 regions that are involved in mPER2 and FBXL3 interactions, as well as transcriptional repression activities of mCRY1 (Czarna et al., 2013). Consistent with our structure-based mutational analyses (Czarna et al., 2013), the mCRY2/FBXL3/SKP1 complex structure (Xing et al., 2013) showed that FBXL3 interacts with the flavin adenine dinucleotide (FAD)-binding pocket, the C-terminal helix α22, and the C-terminal lid of the mCRY-PHR. Moreover, competition with mPER2 or FAD disrupts a preformed mCRY2/FBXL3 complex (Xing et al., 2013), and a period-lengthening small-molecule compound that competes with FAD binding stabilizes mCRY1 by inhibiting ubiquitination (Hirota et al., 2012).

Here, we have determined the crystal structure of the complex between the mCRY1-PHR and a C-terminal mPER2 fragment in order to (1) provide further insights into how alternative binding of mPER2, FBXL3, mCLOCK/BMAL1, or FAD regulates mCRY1 stability and transcriptional repression activity and (2) to advance the development of CRY-stabilizing compounds that affect clock or clock-controlled metabolic functions. mPER2 winds around mCRY1, covering extensive surface areas that significantly overlap with the binding sites of FBXL3 and mCLOCK/BMAL1. Interestingly, our complex structure revealed a jointly coordinated zinc ion that critically stabilizes full-length mCRY1-mPER2 interactions in mammalian cells. Our mutational analyses suggest that (1) formation of the Cys412-Cys363 disulfide bond, which we observed in the apo-mCRY1 structure (Czarna et al., 2013), weakens mCRY1-mPER2 interactions,

and (2) zinc facilitates formation of the reduced state of mCRY1 and stabilizes the mCRY1/mPER2 complex. The regulation of mCRY1-mPER2 interactions by zinc binding and CRY disulfide bond formation/reduction may provide a molecular link between the circadian clock and the cell's metabolic/oxidative state.

RESULTS

Crystal Structure of the Mouse CRYPTOCHROME1-PERIOD2 Complex

Using limited proteolysis, we identified a stable mCRY1/mPER2 core complex comprising the mCRY1-PHR (residues 1 to 496) and mPER2 residues 1132 to 1252 (Figures 1, S1, and S2 available online). We have determined its 2.45 Å crystal structure using molecular replacement with apo-mCRY1 (PDB ID 4K0R [Czarna et al., 2013]) as search model in combination with experimental selenium single-wavelength anomalous dispersion (Se-SAD) phasing (Table S1).

In our mCRY1/mPER2 complex structure, mCRY1 adopts the typical cryptochrome/photolyase fold (Müller and Carell, 2009) with an N-terminal α/β domain, a C-terminal α-helical domain, and a connecting linker region (Figure 1). Superposition of apo-mCRY1 and mCRY1/mPER2 reveals several differences between the two mCRY1 structures, especially in the C-terminal lid, which significantly alters its conformation (see below), the antenna recognition loop, the phosphate-binding loop, the linker region, and the C-terminal helix α22 (Figures S3A–S3D). The other characteristic loops of the 6-4-photolyase/animal cryptochrome family, i.e., the protrusion loop, the α5-α6 loop, and the electron-rich sulfur loop (Hitomi et al., 2009) (Figure S2) do not change significantly upon mPER2 binding.

mPER2 winds around the α-helical domain of mCRY1 (Figure 1B). The crystallized mPER2 fragment comprises five α helices (α1–α5, Ile1138–Thr1198) and a short N-terminal antiparallel β sheet formed by residues 1132–1136 (β1) and part of the cloning overhang of mPER2 (β0). Residues Gly1199 to Glu1214 following helix α5 adopt a well-ordered loop structure. The most C-terminal residues 1215–1252 of the crystallized mPER2[1132–1252] fragment are not seen in the electron density due to conformational disorder (Figures 1, S1B, and S1C). Our CD spectra of the mCRY1[1–496]/mPER2[1132–1252] complex support the high helical content of mCRY1-bound mPER2 in solution. CD spectra of apo-mPER2[1132–1252], however, suggest that unbound mPER2 is significantly less structured (Table S2). We therefore propose that mCRY1 binding induces α-helical folding of the C-terminal mPER2 fragment.

The mCRY1/mPER2 Complex Is Stabilized by Four Interfaces and a Zinc Ion

Several elements of the mCRY1-PHR are involved in mPER2 binding: the C-terminal helix α22 and its preceding connector loop, the C-terminal lid, the sulfur loop, the loop connecting helices α5 and α6, helix α12, and helix α15. Overall, the mCRY1/mPER2 complex buries a 3221 $Å^2$ solvent-accessible surface area.

Helix α22 constitutes a central component of the mCRY1-mPER2 interface. It is embedded between mPER2 helix α3 and the loop region C-terminal to mPER2 α5 ("C-terminal helix interface"; Figures 2A and S1A). Notably, Arg483 and Lys485 (mCRY1 α22) are involved in mPER2 binding and transcriptional repression in mammalian cells (Ozber et al., 2010), as well as in interactions with purified C-terminal mBMAL1 fragments (Czarna et al., 2011). In apo- and mPER2-bound mCRY1, Arg483 forms an intramolecular salt bridge with Asp321 (sulfur loop), which likely contributes to positioning of α22 (Figure S3C). In the mCRY1/mPER2 complex, Arg483 forms an additional salt bridge to Asp1167 (mPER2 α3) (Figures 2A, right, and S3C). Furthermore, Gln486 and Gln490 (α22) hydrogen bond to $Gln1168_{mPER2}$, and Gln486 also hydrogen bonds to the backbone of $Leu1164_{mPER2}$ (Figure 2A, left). The sulfur loop further stabilizes the position of mPER2 α3, mostly via hydrophobic interactions of $Pro319_{mCRY1}$ (Figures 2A, right, and S1A). On the other side of mCRY1 α22, Lys485 forms a hydrophilic side-chain interaction with Asp1206 and a backbone hydrogen bond with Val1207 in the C-terminal mPER2 loop region (Figure 2A, left).

Notably, Cys1210 and Cys1213 in the C-terminal mPER2 loop region and mCRY1 residues Cys414 (lid) and His473 (α22) tetrahedrally coordinate a zinc ion ("zinc interface"; Figures 1B, 2B, S1A, and S4). An anomalous difference map calculated for positioning of the selenomethionines of mPER2 gave first evidence for the zinc ion in the crystal (Figures S4A and S4B). An X-ray fluorescence scan confirmed its presence (Figure S4C). Atomic absorption spectroscopy confirmed the presence of zinc in the mCRY1/mPER2 complex in solution, but not in the single proteins due to their incomplete zinc-binding sites (Figure S4D).

Another heterodimer interface is formed between mCRY1 α12 and mPER2 helices α1 and α2 (referred to as "mPER2(α1-2)-mCRY1(α12) interface"; Figures 2C and S1A). mPER2 α1 additionally contacts mCRY1 α15, whereas mPER2 α2 also interfaces with Tyr466 to Met470 in the loop preceding mCRY1 α22. Trp1139 (mPER2 α1) contacts mCRY1 α12 and α15. Lys329 (mCRY1 α12) hydrogen bonds to backbone oxygens of Ile1149 to Tyr1153 (mPER2 α2) and Asn323 to the Tyr1153 side chain. The loop connecting mPER2 α1 and α2 winds tightly around Ala328 of mCRY1 α12.

mPER2 α4, which is part of a 20 amino acid stretch (1179 to 1198) reported to be essential for mCRY1 binding in cell-based assays (Tomita et al., 2010), packs against the C-terminal lid (including Phe405) and the α5–α6 connector loop (including Leu148 and Thr149) of mCRY1 ("mPER2(α4)-cap interface"; Figures 2D and S1A). Leu148 makes hydrophobic interactions with Leu1189 and Phe1181 of mPER2, whereas Thr149 hydrogen bonds to Glu1188 and (water mediated) to Glu1191 of mPER2 α4.

The mCRY C-Terminal Lid Adopts Variable Conformations and Is Involved in Disulfide Bond Formation and Zinc Coordination

The major difference between the apo-mCRY1 and mCRY1 complex structure manifests in the conformation of the C-terminal lid. Although the side chains of residues Phe406 to Phe410 are disordered in the apo structure, the loop is well defined and adopts a deviating orientation in the complex structure (Figure 3A). This is likely due to its packing against α4, α5, and the C-terminal loop of mPER2 (Figures 1B, 2D, 3B, and S3D). The

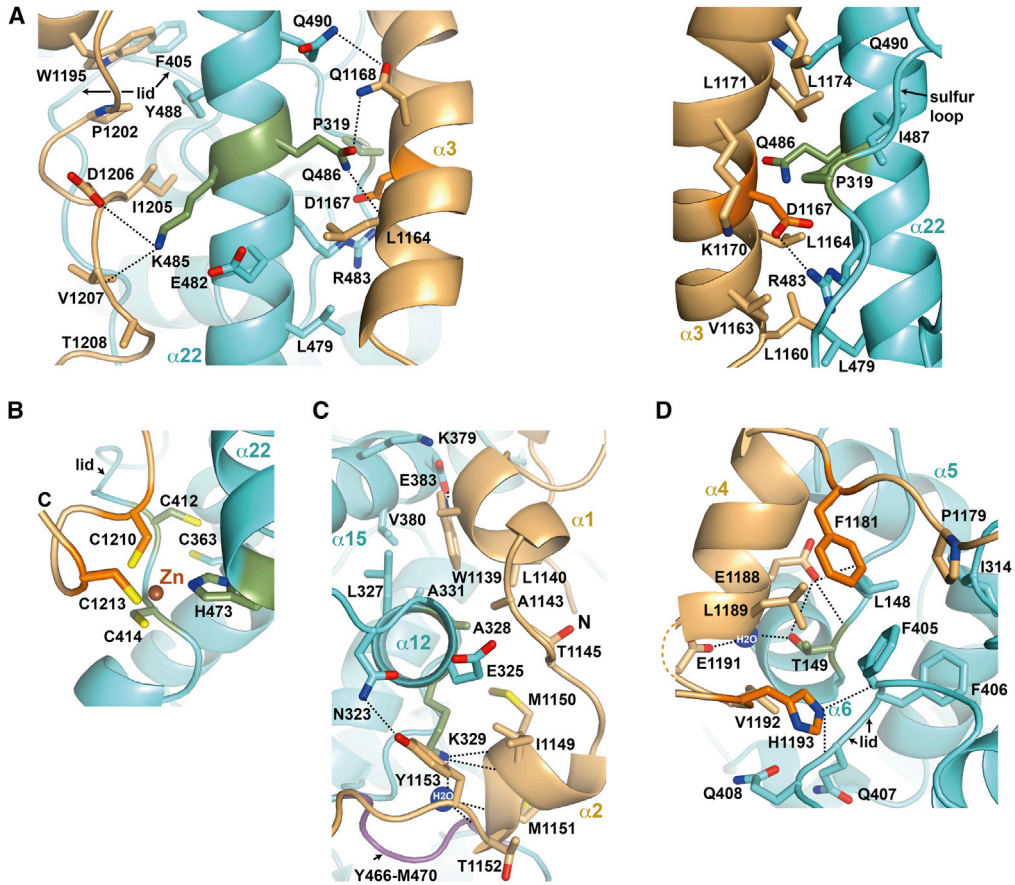

Figure 2. Close-Up View of mCRY1-mPER2 Interfaces

Crucial interface residues are shown as atomic sticks. Mutated residues are highlighted in green (CRY) and orange (PER). Dashed lines indicate salt bridges and hydrogen bonds. See Results and Figure S1A legend for a detailed description of the interactions.

(A) C-terminal helix (α22) interface, two orientations: mCRY1 α22 is clenched by mPER2 helix α3 and the loop connecting mPER2 α5 with the zinc binding motif.

(B) Zinc (Zn) interface: His473 (α22) and Cys414 (lid) of mCRY1 and Cys1210 and Cys1213 of mPER2 tetrahedrally coordinate a zinc ion. The disulfide bridge between Cys363 and Cys412 (compare apo-mCRY1; Figures 3A and 3B) is broken. This figure directly connects to Figure 2A (left) (compare Thr1208 [A] and Cys1210 [B]).

(C) mPER2(α1–2)-mCRY1(α12) interface: mPER2 helices α1 and α2 interact with mCRY1 helices α12 and α15 and with Tyr466-Met470 in the loop preceding α22.

(D) mPER2(α4)-cap interface: mPER2 helix α4 packs against Thr149 and Leu148 in the α5-α6 loop and the C-terminal lid of mCRY1.

See also Figures S1, S2, S3, and S4.

apo-mCRY1 structure contains a disulfide bridge between Cys363 and Cys412, which has the potential to be a redox-dependent link to the FAD-binding pocket (Czarna et al., 2013). Located in the immediate vicinity of the zinc interface, this disulfide bridge is broken in the complex structure (Figures 2B and 3). Thereby, we hypothesize that the C-terminal lid gains a higher flexibility for interaction with mPER2.

In apo-mCRY1, Phe405 is embedded in a hydrophobic pocket of the mCRY1-PHR. In the mCRY1/mPER2 complex, however, Phe406 occupies the hydrophobic pocket of apo-Phe405, whereas Phe405 projects to the surface (Figure 3A) and embeds into a huge hydrophobic pocket lined by PER and CRY residues (Figures 2D, S1A, and S3D). The mPER2-bound lid conformation is additionally stabilized by backbone hydrogen bonding of Phe405 and Gln407 with $His1193_{mPER2}$ (Figure 2D) and by Phe410, which inserts into a hydrophobic pocket, including His359 and Trp399 (Figure 3B).

In apo- and FBXL3-bound mCRY2 (Xing et al., 2013), the lid adopts yet another position than in apo- and mPER2-bound mCRY1. Phe424 and Phe423 of mCRY2/FBXL3 (Figure 3C) and apo-mCRY2 (data not shown) position just as the corresponding Phe406 and Phe405 in apo-mCRY1. $Phe428_{mCRY2}$ (corresponding to $Phe410_{mCRY1}$) is not embedded in the mCRY-PHR but is turned away from the mCRY2 core and mediates interactions with FBXL3. Interestingly, in both the apo-mCRY2- and the mCRY2/FBXL3 complex structure, there is no disulfide bridge between Cys381 and Cys430 (corresponding to Cys363 and Cys412 in mCRY1) (Figures 3C, S3E, and S3F). Instead, Cys430 forms an intermolecular disulfide bridge with Cys340 of FBXL3 in the mCRY2/FBXL3 complex structure (Figure S3F).

The FAD-Binding Pocket of mCRY1

The mCRY2/FBXL3/SKP1 complex structure (Xing et al., 2013) revealed that the C-terminal tail of FBXL3 occupies the FAD-binding

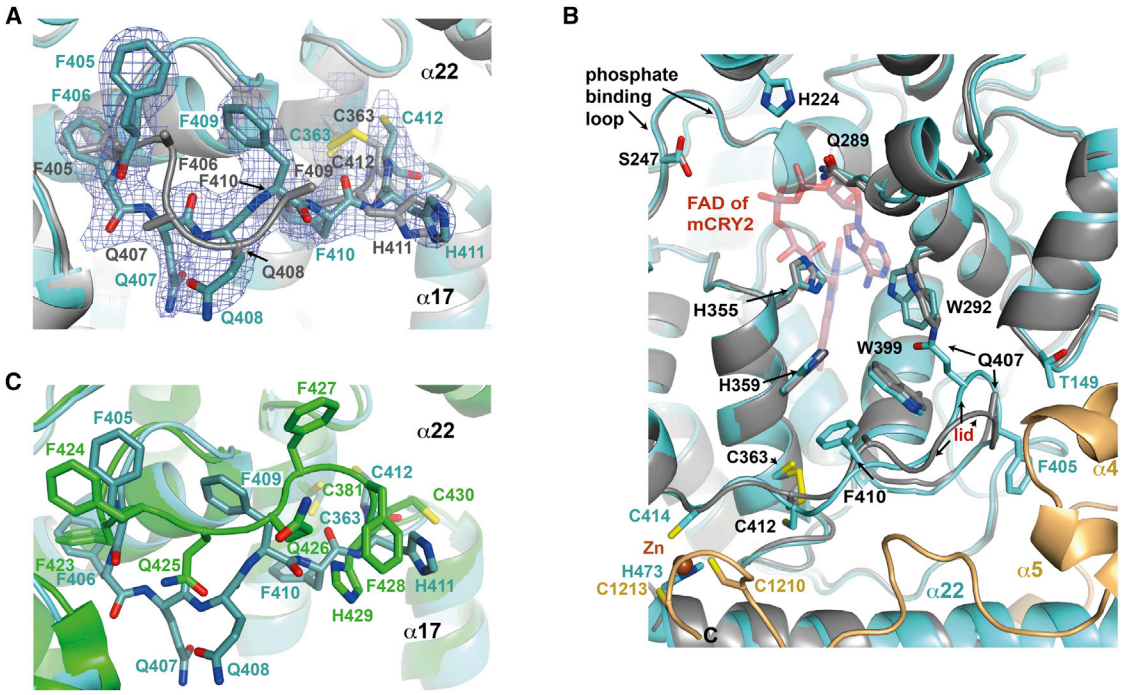

Figure 3. C-Terminal Lid and FAD-Binding Pocket of the mCRY1/mPER2 Complex

(A–C) The C-terminal lid adopts varying conformations in apo-CRY1, the mCRY1/mPER2 complex, and mCRY2. See Results for detailed comparison.

(A) Superposed C-terminal lids of mPER2-bound mCRY1 (cyan, mPER2 not shown) and apo-mCRY1 (gray). Apo-mCRY1: Phe406 to Phe410 are built as alanine. mPER2-bound mCRY1: Phe406 adopts the position of apo-Phe405 whereas Phe405 points away from the mCRY1-PHR. The Cys363-Cys412 disulfide bridge is broken. The 2Fo-Fc electron density (1σ level) of complex mCRY1 is shown in blue.

(B) Superposition of FAD-binding pocket, C-terminal lid, and zinc-interface of the mCRY1/mPER2 complex (cyan/yellow) with apo-mCRY1 (gray) and FAD from the mCRY2/FAD complex (Xing et al., 2013) (red, taken from PDB ID 4I6G; mCRY2 protein not shown for clarity). Upon mPER2 binding, the C-terminal lid and its Gln407 side chain reorient. Trp292 rotates such that it would interfere with FAD binding.

(C) Superposition of C-terminal lids of mPER2-bound mCRY1 (cyan, mPER2 not shown) and FBXL3-bound mCRY2 (green, FBXL3 not shown). The disulfide bridge between Cys381 and Cys430 (corresponding to Cys363-Cys412 of apo-mCRY1) is not observed in mCRY2 (see also Figures S3E and S3F).

See also Figure S3.

pocket of mCRY2. In our mCRY1/mPER2 complex structure, however, the FAD-binding pocket is accessible, unoccupied, and in a very similar conformation as in apo-mCRY1 (Figure 3B) and apo-mCRY2. Notably, the side chains of Gln289, Trp292, and His355 adopt an introversive position, which would interfere with FAD binding. mPER2 binding does not affect the conformation of His355 and Gln289, but reorientation of Trp292 is required to allow for the positioning of Gln407 in the mPER2-bound lid conformation. We therefore suggest that, although mPER2 binding to mCRY1 may somewhat negatively affect FAD binding by enforcing an unfavorable side-chain orientation of Trp292, it neither requires nor fully excludes the presence of FAD.

Structural Basis for Mutually Exclusive Binding of mPER2 and FBXL3 to mCRY

Our mCRY1/mPER2 crystal structure explains why mPER2-bound mCRY2 is completely devoid of FBXL3 in HEK293 cells and a purified C-terminal mPER2 fragment displaces mCRY2 from FBXL3 (Xing et al., 2013) (Figure 4). Whereas mPER2 α3 blocks binding of the leucine-rich repeat (LRR) N domain of FBXL3 to helix α22 and the sulfur loop of mCRY (Figure 4B, left), the C-terminal mPER2 loop region, including the zinc interface, interferes with binding of the LRR C domain of FBXL3 to mCRY α22 and the lid (Figure 4B, right). Moreover, mPER2 α4 and α5 completely overlap with the conserved mCRY2 C-terminal extension sequence (CCS), implying that the CCS adopts a deviating orientation in the mCRY1/mPER2 complex (Figure 4B, right).

The high sequence identity (86%) and conservation of mCRY binding residues between FBXL3 and FBXL21 (Hirano et al., 2013; Yoo et al., 2013) suggest that these two counteracting E3-ligase subunits bind to the same mCRY surface regions, and therefore, simultaneous binding of FBXL21 and mPER2 is unlikely, too.

Analyses of mCRY1-mPER2 Interactions In Vitro

To validate our mCRY1/mPER2 complex structure in solution and to assess the relative contributions of the different interfaces in vitro, we have generated mPER2[1119–1252] fragments with point mutations in the mCRY1/mPER2 interfaces. Effects of these mutations on the mCRY1-mPER2 interaction were analyzed in pull-down assays using total lysates and in native gels using purified proteins (Figures 5A, 5C, and 5D). The single H1193E mutation in the mPER2(α4)-cap interface, which aims to

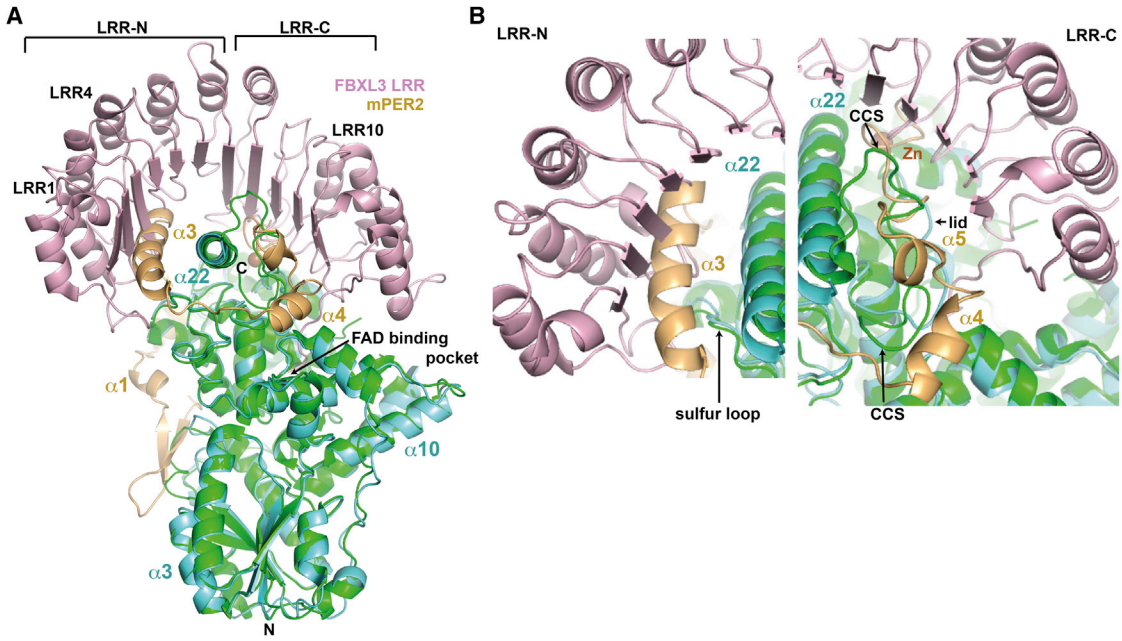

Figure 4. mPER2 and FBXL3 LRR Are Mutually Exclusive in Binding to mCRY1/2

(A) Superposition of mCRY1 (cyan) in complex with mPER2 (yellow) and mCRY2 (green) in complex with FBXL3 LRR (leucine-rich repeat domain, light pink; PDB ID 4I6J) (rmsd = 2.047 Å for 486 CRY Cα positions).

(B) Close-up view: mPER2[1132–1252] and FBXL3 LRR occupy partly overlapping binding sites on mCRY (CCS, conserved cryptochrome C-terminal extension sequence).

See also Figure S3.

electrostatically interfere with binding to the mCRY1 C-terminal lid (Figure 2D), showed wild-type (WT)-like behavior in both assays. However, in combination with the D1167R mutation in the C-terminal helix interface (Figure 2A, right), the H1193E mutation further weakens mCRY1 binding. Binding of mCRY1 was even more severely impaired through the additional F1181R mutation, which also targets the interaction with the mCRY1 C-terminal lid (Figure 2D). These results suggest that both interfaces (C-terminal helix interface and mPER2(α4)-cap interface) are of similar importance for complex formation in vitro. In addition, our native gel analyses imply that the mCRY1 tail is not required for mCRY1/mPER2 complex formation, as comparable results were gained with the mCRY1-PHR and full-length mCRY1 (Figures 5C and 5D).

Mutation of the zinc-coordinating residues Cys1210 and Cys1213 to alanine surprisingly did not compromise complex formation in vitro, neither in the total lysate (natural presence of zinc) nor in the purified system (supplied with zinc acetate) (Figures 5A, 5C, and 5D). Furthermore, no difference in complex formation was observed for WT proteins whether zinc was added to the buffer or not (Figures 5C and 5D), implying that the zinc-binding interface is of minor importance for complex formation in vitro. Affinity measurements (isothermal titration calorimetry, ITC) further support this result because a K_d in the lower nanomolar range was observed for the mCRY1-mPER2 interaction even in the absence of zinc ions (Figure 5B). However, zinc binding clearly stabilizes the purified mCRY1/mPER2 complex as demonstrated by the higher melting temperature of the WT complex compared to the zinc-free mCRY1/mPER2(C1210A/C1213A) mutant complex in our thermofluor experiments (Figure 6A). Furthermore, ITC experiments revealed that the WT mCRY1/mPER2 complex binds zinc ions with a nanomolar affinity (K_d of ~8 nM) (Figure 6B).

mCRY1-mPER2 Heterodimer Interfaces Are Present in a Cellular Context

To validate our mCRY1/mPER2 complex structure in a cellular environment and in the context of full-length mCRY1 and mPER2 proteins, we have tested mCRY1 interface mutants for their effect on the stability of the mCRY1/mPER2 complex using a luciferase complementation assay (Figures 7A and S5A). Full-length mCRY1 and mPER2 (WT or mutants) were expressed as fusion proteins with C- and N-terminal firefly luciferase fragments in HEK293 cells (Czarna et al., 2013). mPER2-mCRY1 interactions lead to a functional luciferase whose activity was measured in cell lysates.

The mCRY1 T149E mutation was designed to sterically and electrostatically weaken interactions with mPER2 α4 (Figure 2D). Consistent with our structure and the reported importance of mPER2 helices α4 and α5 for mCRY-mPER interactions (Tomita et al., 2010), the T149E mutation drastically reduced mPER2 binding.

Disruption of the interaction of mCRY1 α22 with mPER2 α3 (Q486R) and with the loop connecting mPER2 α5 with the zinc-binding motif (K485D) (Figure 2A, K485D/Q486R double mutant) drastically reduced mPER2 binding to below 10%. This confirms

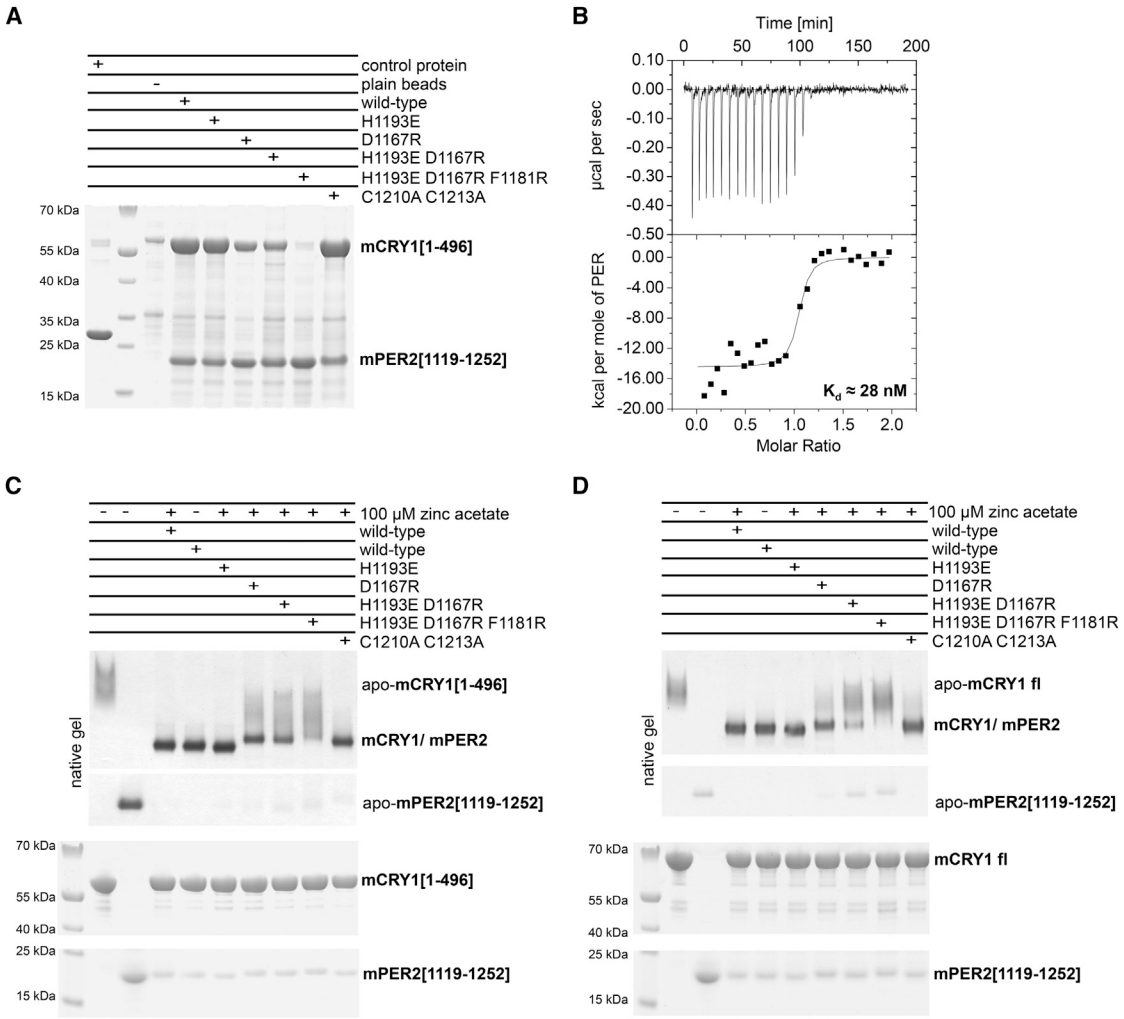

Figure 5. Biochemical Analysis of mCRY1/mPER2 Interfaces

(A) Ni^{2+} pull-down from total cell lysates testing for interactions of N-terminally His-tagged WT and mutant mPER2[1119–1252] proteins with untagged mCRY1 [1–496]. Eluates were analyzed on a Coomassie-stained 18% SDS-PAA gel. Negative controls: lane 1, pull-down of mCRY1 with a noncircadian control protein; lane 3, pull-down with plain beads.

(B) ITC profile for the interaction of mCRY1[1–496] and mPER2[1119–1252]. The binding event is exothermic. Top: time response of heat change upon addition of ligand (mPER2). Bottom: best fit obtained with a single site-binding model (best χ^2 statistic), resulting in a 1:1 stoichiometry (n = 1.02). The approximate K_d for the mCRY1-mPER2 interaction is 28 nM.

(C and D) Native gels (top) with purified proteins testing interactions of mPER2[1119–1252] (WT and mutants) with (C) mCRY1[1–496] (PHR) and (D) mCRY1 [1–606] (full length). Samples were also analyzed by SDS-PAGE (bottom).

See also Figure S1 and Table S2.

the existence and importance of the combined C-terminal helix interface in a cellular environment. The P319R mutation in the mCRY1 sulfur loop should also weaken the interaction with mPER2 α3 (Figure 2A). Whereas the P319R mutation moderately reduced binding in our luciferase complementation assay (this study), the K485D single mutation reduced binding to ~20% (Czarna et al., 2013). This finding suggests that mCRY1 binding to the mPER2 loop region (targeted by K485D) is more important than the interaction with the long mPER2 helix α3 (targeted by Q486R and P319R) in vivo.

A double mutation in the mPER2(α1–2)-mCRY1(α12) interface (A328R/K329D) (Figure 2C) reduces mPER2 interactions by about one half. We conclude that mPER2 helices α1 and α2 contribute to mCRY1 binding also in a cellular environment but are not as important for complex stability as for example helix α4.

Zinc Binding and Adjacent Disulfide Bond Formation Are Interdependent in a Cellular Context and In Vitro

To define potential roles of the zinc ion and the CRY1 Cys363-Cys412 disulfide bridge in a cellular environment, we have mutated the zinc-coordinating residues of mCRY1 (Cys414 and His473) and mPER2 (Cys1210 and Cys1213), as well as Cys363 and Cys412 to alanine. The mutants were tested for their effect on the stability of the mCRY1/mPER2 complex using a

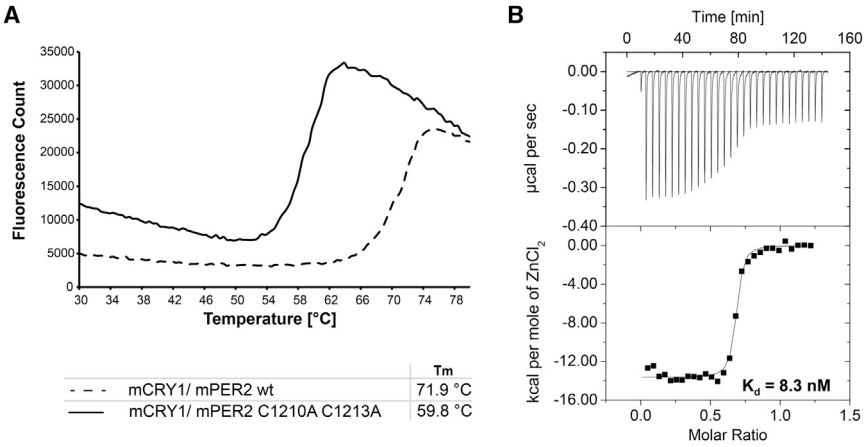

Figure 6. High-Affinity Zinc Binding Stabilizes the mCRY1-mPER2 Complex

(A) Melting temperature determination by thermofluor analysis of zinc-stabilized WT mCRY1 [1–496]/mPER2[1119–1252] complex in comparison with zinc-free mCRY1/mPER2(C1210A C1213A) mutant complex.

(B) ITC profile of zinc binding to the mCRY1 [1–496]/mPER2[1119–1252] complex. The binding event is exothermic. Top: time response of heat change upon addition of the zinc ligand. Bottom: best fit obtained with a single site-binding model (best χ^2 statistic) results in a stoichiometry of n = 0.67, probably because not all complexes are active in zinc binding. The approximate K_d for Zn^{2+} binding to the mCRY1/mPER2 complex is 8 nM. See also Figures S4, S6, and S7.

luciferase complementation assay in HEK293 cells (Figures 7A and S5A).

The mCRY1 single mutations C414A and H473A significantly reduced mPER2 binding, with the C414A single mutation being more effective. Furthermore, very weak interactions were observed between the mPER2(C1210A/C1213A) double-mutant protein and wild-type or C414A mutant mCRY1, indicating that zinc coordination is of vital importance for the formation of a stable complex between full-length mCRY1 and mPER2 in vivo.

C412A and C363A single mutations, which prevent formation of the Cys412-Cys363 disulfide bridge, slightly enhanced mPER2 binding in some of our luciferase complementation assays yet behaved wild-type like in other experiments. We propose that disruption of this disulfide bridge enhances mPER2 binding by facilitating the observed conformational changes of the mCRY1 lid (discussed above). The mild and somewhat fluctuating impact of the C412A and C363A single mutations on mPER2 binding probably depends on the redox status and hence the extent of Cys412-Cys363 disulfide bridge formation in the HEK293 cells.

To test whether mCRY1 exists in an oxidized form also in living cells, we analyzed mCRY1 disulfide bridge formation in HEK293 cells by N-Ethylmaleimide (NEM) and Maleimide-PEG (MP) modification (Figure 7B). Indeed, we found increased molecular weight forms of mCRY1 (CRY1-MP) only in lysates that were dithiothreitol (DTT) treated before MP modification, but not when lysates were either left untreated or when potential disulfide bridges were stabilized with H_2O_2. This indicates that full-length mCRY1 also occurs in oxidized forms within cells.

Quite surprisingly, the mCRY1 C414A/C412A and the C414A/C363A double mutations only weakened mPER2 binding to ~50% in our luciferase complementation assay (Figure 7A). Furthermore, mCRY1 single- (C412A) or double (C412A/C414A)-mutant proteins showed ~50% binding activity toward mPER2 proteins containing the C1210A/C1213A double mutation. Hence, the C412A and C363A mutations partially rescue the severe weakening of the mCRY1-mPER2 interaction by the mCRY1 (C414A) and mPER2 (C1210A/C1213A) mutations, suggesting that reduction of the Cys412-Cys363 disulfide bridge and the resulting increased flexibility of the mCRY1 C-terminal lid decrease the severity of disruption of the zinc-binding site.

To further elucidate whether the mCRY1 Cys412-Cys363 disulfide bridge forms in dependence of zinc in the mCRY1/mPER2 complex in vitro, we kept purified zinc-containing and zinc-free mCRY1/mPER2 complexes under reducing or nonreducing conditions and monitored the mCRY1 oxidation status by mass spectrometry (MS) (Figure S6). The presence of zinc in the complexes was analyzed in parallel by atomic absorption spectroscopy (ICP-OES) (Figure S7). Under nonreducing conditions, only a moderate amount of the putatively oxidized mCRY1 species (with the total mass reduced by ~2 Da as expected for the oxidation of a disulfide bridge) is observed in the zinc-bound WT mCRY1/mPER2 complex (Figure S6A, middle). However, in the zinc-free mCRY1/mPER2(C1210A/C1213A) mutant complex (Figure S6B), as well as when the zinc ion is removed from the WT complex through EDTA (Figure S6A, right), mCRY1 appears almost completely oxidized. To test whether the mCRY1 oxidation status is affected by disulfide bond formation between Cys412 and Cys363, we mutated Cys412 to alanine. Indeed, the C412A mutation substantially reduced mCRY1 oxidation in the zinc-free mCRY1(C412A)/mPER2(C1210A/C1213A) mutant complex (Figure S6C), indicating that Cys412 oxidation accounts for a significant fraction of the MS peak CRY_{p1} assigned to oxidized mCRY1 protein. However, we also found a moderate amount of putatively oxidized mCRY1 after aeration in the C412A mutant, suggesting additional disulfide bond formation (Figure S6C). Notably, the behavior of the purified zinc-free mCRY1(C412A)/mPER2(C1210A/C1213A) complex mirrors that of the WT mCRY1/mPER2 complex in our MS experiments (Figure S6D). This observation is consistent with the partial rescue of zinc-binding deficiency by the C412A and C363A mutations observed in our luciferase complementation experiment (Figure 7A).

In conclusion, our mutational analyses confirm the presence of all heterodimer interfaces revealed by our mCRY1/mPER2 crystal structure and indicate an interdependent role of the coordinated zinc ion and of the mCRY1 Cys412-Cys363 disulfide bridge, among others, in the positive (zinc) and negative (disulfide bridge) regulation of the mCRY1-mPER2 interaction in vivo.

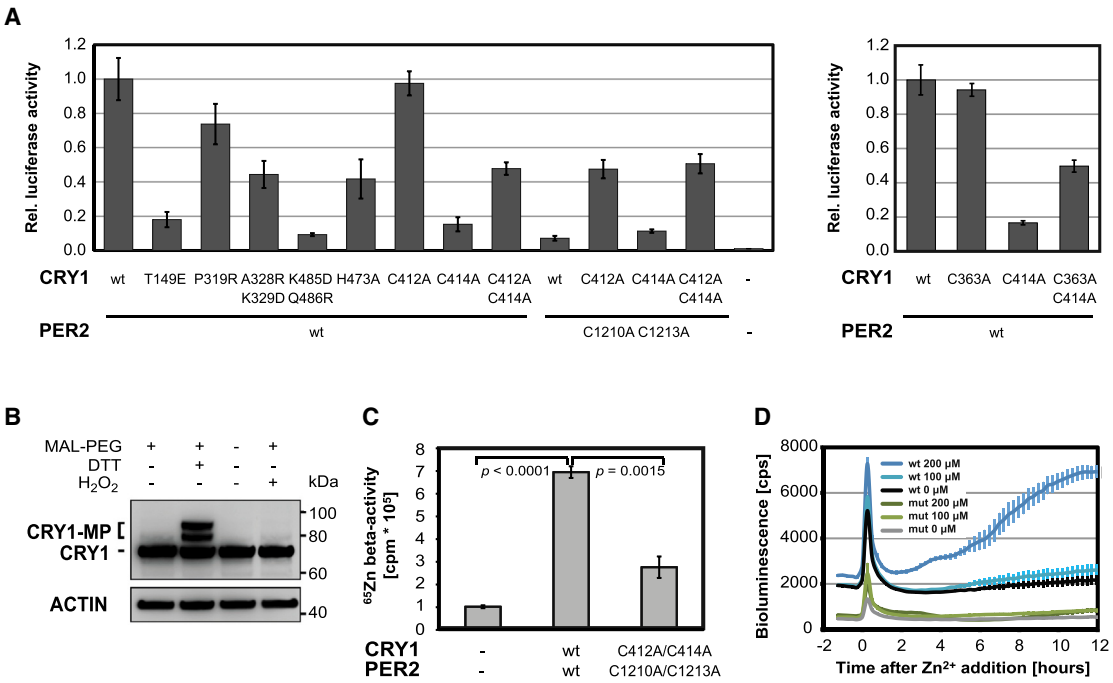

Figure 7. mCRY1/mPER2 Complex Formation Is Regulated by Four Interfaces, a Zinc Ion, and Disulfide Bridge Formation in Living Cells

(A) Luciferase complementation assay. All heterodimer interfaces revealed by the crystal structure are present in full-length mCRY1/mPER2 complexes inside cells. Disruption of the zinc interface is partially rescued by mutation of the disulfide bond forming Cys363 and Cys412. Full-length mCRY1 and mPER2 (WT or mutants) were expressed as fusion proteins with firefly luciferase fragments in HEK293 cells (Czarna et al., 2013). Approximately equal expression of fusion proteins was detected in western blot experiments (Figure S5A). Data are normalized to renilla luciferase activity (used as a transfection control) and presented relative to mCRY1(WT)-mPER2(WT) activity. Shown are mean ± SEM of three (left) or four (right) independent transfections. Three additional experiments gave similar results.

(B) mCRY1 forms disulfide bridges in living cells: HEK293 cells transiently transfected with mCRY1 were harvested in presence of excess amounts of N-Ethylmaleimide (NEM) that immediately block all free thiol groups. Subsequently, disulfide bridges were reduced with Dithiothreitol (+DTT), and any thiol group previously oxidized was now modified with Maleimide-PEG (MP, MW 5 kDa). Increased molecular-weight forms of mCRY1 were detected in cell lysates treated with DTT, but not when lysates were not reduced (−DTT) or even oxidized with H_2O_2. This indicates that, within cells, full-length mCRY1 can occur in oxidized forms with one or more disulfide bridges.

(C) Critical cysteine residues coordinate zinc in the mCRY1/mPER2 complex in a cellular context: HEK293 cells were transiently transfected with full-length mPER2 or mCRY1 either as WT versions or with alanine mutations in the zinc-coordinating Cys414 (mCRY1), Cys1210, and Cys1213 (mPER2), as well as the disulfide bond forming Cys412 of mCRY1. Immunoprecipitated mPER2 was incubated with mCRY1-containing cell lysate in the presence of the radioactive zinc isotope $^{65}Zn^{2+}$. In this pull-down assay, WT proteins incorporated significantly (t test) more $^{65}Zn^{2+}$ than the mutants. Shown are mean ± SEM of three independent immunoprecipitation experiments. The high expression of proteins was verified in western blot experiments (not shown).

(D) Zinc ions enhance the mCRY1-mPER2 interaction in living cells: Two U2-OS reporter cell lines, which stably express mCRY1 and mPER2 split luciferase fusion proteins either as WT or with alanine mutations in the zinc-coordinating cysteins (Cys414 of mCRY1; Cys1210, Cys1213 of mPER2) and Cys412 of mCRY1 (mut: C412A/C414A/C1210A/C1213A), were cultivated in Zn^{2+}-depleted medium for about a week. Then various concentrations of Zn^{2+} were added to the medium while continuously monitoring luciferase activity. Treatment with zinc ions (but not iron ions, not shown) dose-dependently increases luciferase activity in cells expressing WT mCRY1 and mPER2 (see also Figure S5C), but not or to a much lesser extent in cells expressing mCRY1 and mPER2 with mutations of zinc-coordinating residues. Zinc has no effect on mRNA expression levels of the reporter constructs (not shown) or on luciferase activity of a control U2-OS cell expressing mCRY1-LUCIFERASE (not shown). Shown are mean ± SEM of four independent treatments. Several additional experiments gave similar results.

See also Figures S1, S2, and S5.

Zinc Ions Bind to the mCRY1/mPER2 Complex in a Cellular Context and Enhance the mCRY1-mPER2 Interaction in Living Cells

To test whether zinc can bind to the mCRY1/mPER2 complex in a cellular environment, we transiently transfected HEK293 cells with full-length mPER2 or full-length mCRY1 either as WT versions or with mutations in the three zinc-coordinating cysteines (mCRY1: C414A; mPER2: C1210A and C1213A) and the disulfide bridge forming Cys412 of mCRY1. To ensure that sufficiently stable mCRY1/mPER2 complexes are formed even without zinc coordination, we used the mCRY1 (C412A and C414A) double mutant, which enhanced mCRY1-mPER2 interaction compared to the C414A single mutation in our luciferase complementation assays (Figure 7A). Immunoprecipitated mPER2 was incubated with mCRY1-containing cell lysate in the presence of the radioactive zinc isotope $^{65}Zn^{2+}$. A 7-fold increase in $^{65}Zn^{2+}$ radioactivity was detected when mPER2- and mCRY1-containing cell lysates were used. Mutations in the zinc coordination site led to a substantial and significant reduction of zinc binding (Figure 7C). In addition, immunoprecipitated mPER2 incubated with a control lysate did essentially not incorporate $^{65}Zn^{2+}$ (Figure S5B). Together, these results indicate

that zinc can bind to the full-length mCRY1/mPER2 complex in a cellular context, and this binding depends on critical zinc-coordinating cysteine residues in both proteins. The residual radioactivity observed for the mutant proteins could be due to $^{65}Zn^{2+}$ binding to large endogenous mCRY1/mPER2 complexes recruited via mPER PAS domain homodimer interactions (Kucera et al., 2012), as well as unspecific zinc binding.

To investigate whether zinc ions also contribute to the stabilization of the mCRY1-mPER2 interaction in living cells, we created two reporter U2-OS cell lines that stably express mPER2 and mCRY1 split luciferase fusion proteins either as WT proteins or with mutations in the zinc-coordinating residues Cys414 (mCRY1), Cys1210, and Cys1213 (mPER2), as well as the disulfide bridge forming Cys412 of mCRY1 (mut: C412A/C414A/C1210A/C1213A). Treatment with zinc (but not iron) ions dose-dependently enhances the bioluminescence in cells expressing WT mPER2 and mCRY1, but not or to a much lesser extent in cells expressing mutant mCRY1 and mPER2 proteins, indicating that zinc coordination indeed contributes to mCRY1-mPER2 interaction strength, and this effect depends on the integrity of the zinc-coordinating residues (Figures 7D and S5C).

DISCUSSION

Our crystal structure of the mCRY1/mPER2 heterodimer shows an intimate and high-affinity clock protein complex with a zinc interface that critically stabilizes the mCRY1/mPER2 complex in mammalian cells. Our cell-based and in vitro (LC-ESI-MS/ICP-OES) studies suggest that the coordinated zinc ion structurally facilitates the reduction of a nearby located disulfide bridge of mCRY1 (probably between Cys412 and Cys363, among others), which likely enhances the flexibility of the mCRY1 C-terminal lid and thereby mPER2 binding. This functionally important interplay between an intermolecular composite 3Cys/1His zinc-binding site in a heterodimer interface and one or more intramolecular disulfide bonds formed by nearby located cysteine residues has not been observed in other zinc-binding proteins (e.g., Maret, 2012; Auld, 2001). Notably, the redox-regulated chaperone Hsp33 and anti-σ factor RsrA use intramolecular cysteine-containing zinc centers as redox sensors (Ilbert et al., 2006). In both proteins, oxidative or disulfide stress leads to oxidation and, hence, disulfide bond formation of their zinc-coordinating cysteines, as well as zinc release, which induce conformational changes leading to their functional activation. On the other hand, betaine-homocysteine methyltransferase is reversibly inactivated through oxidation of its zinc-coordinating cysteines and zinc release (Evans et al., 2002).

Our LC-ESI-MS/ICP-OES experiments show that the mCRY1/mPER2 complex does not release its zinc ion under nonreducing conditions (Figure S7, number 2). Instead, the experiments suggest that zinc release supports mCRY1 oxidation (Figures S6A, top right, and S6B) and that this oxidation also involves Cys412 (Figure S6C). Using the same basic elements (i.e., a zinc ion and a nearby located highly reactive cysteine) but in a different structural arrangement, mode of action, and interplay, the CRY1/PER2 complex therefore may act as a sensor of the rhythmically changing redox state of the cell, which was proposed to be involved in driving circadian rhythms (Edgar et al., 2012; O'Neill and Reddy, 2011; O'Neill et al., 2011; Wang et al., 2012).

In general, there are various intracellular zinc pools described such as zinc in vesicles, zinc tightly bound to macromolecules, zinc bound to metallothioneins (the major cellular zinc storage proteins), and a pool of "free" zinc (Oteiza, 2012). Although the total cellular amount of zinc is described to be in the high micromolar range, the concentration of "free" zinc is much lower (nano- to picomolar) because most zinc is bound to proteins with high affinity. However, under certain circumstances, e.g., oxidative stress, zinc may be released. Our measured K_d for zinc binding to the mCRY1/mPER2 complex in the lower nanomolar range suggests a dynamic, regulatory zinc-binding site that might be influenced by its environment within the cell.

Interestingly, the zinc-coordinating residues and most other residues mediating CRY-PER interactions are conserved in vertebrate CRY and PER2 proteins, in PER1, and, to a minor extent, in PER3, which strongly suggests the existence of homologous CRY/PER complexes (Figures S1 and S2).

Lacking the knowledge about the mCRY1-mPER2 zinc interface, Okano et al. (2009) generated a transgenic mouse line constitutively overexpressing mCRY1 with a C414A mutation. These mice showed a long 28 hr free-running period of locomotor activity rhythms and abnormal entrainment behavior, as well as symptoms of diabetes, including reduced β cell proliferation and insulin secretion (hypoinsulinemia) (Okano et al., 2009, 2010, 2013). Most likely, these dominant in vivo effects of the C414A mutation are due to disruption of the mCRY1-mPER2 zinc interface, demonstrating the importance of zinc-dependent mCRY1/mPER2 complex formation for circadian dynamics and metabolic regulation. Notably, mutations in mBMAL1 and mCLOCK also lead to hypoinsulinemia and defective β cell function, whereas mCRY1/mCRY2 double-knockout mice exhibit hyperinsulinemia and tissue-specific insulin resistance (Barclay et al., 2013; Marcheva et al., 2010). Furthermore, the mCLOCKΔ19 mutation leads to extended circadian periods, whereas *mCry1*$^{-/-}$ mice exhibit a period shortened by 1 hr (King et al., 1997; van der Horst et al., 1999). Hence, the circadian and metabolic phenotypes of the mCRY1 C414A mutation are more similar to those resulting from mutations in the mCLOCK/BMAL1 complex than to mCRY knockouts. Our structure suggests that the intimate interaction of mPER2 with mCRY1 α22 interferes with repressive mCRY1 binding to the mCLOCK/BMAL1-E-box complex. Thus, we speculate that the weakened mPER2 interaction of the zinc-binding-deficient mCRY1(C414A) mutant protein (Figure 7A) leads to an enhanced transcriptional repression activity in vivo. We further propose that, in transgenic mice, the overexpressed mCRY1(C414A) mutant protein represses the mCLOCK/BMAL1 complex more strongly than endogenous WT mCRY1. This may cause the dominant phenotype of the mCRY1(C414A) mutation, which somewhat resembles the phenotypes of transgenic mice expressing weakened transcriptional activator complexes, including, for example, the mCLOCKΔ19 mutant protein.

Our structure also shows that binding of FBXL3 or PER2 to CRY is mutually exclusive and suggests that PER2 stabilizes

CRY1 by shielding it from FBXL3. Strikingly, neither mPER2 (this study) nor FBXL3 (Xing et al., 2013) binds in close proximity of the AMPK phosphorylation site Ser71, suggesting that AMPK regulates PER2 and FBXL3 binding in a more indirect manner. Notably, Cys412 appears highly reactive in switching functions because it not only forms the intramolecular disulfide bond to Cys363 in apo-mCRY1 but also an intermolecular disulfide bond with FBXL3 in the CRY2/FBXL3 complex structure.

Taken together, our crystal structure provides a more complete understanding of how mammalian CRY and PER proteins interact, how this interaction might be sensing and be regulated by cellular redox/metabolic states, and how the interplay with other clock components drives the circadian clock and metabolic processes. This will guide the design of new mutants, experiments, and small-molecule ligands to study or target macromolecular CRY/PER containing complexes in vivo.

EXPERIMENTAL PROCEDURES

Protein Purification and Crystallization

mCRY1 and mPER2 proteins were recombinantly expressed as His-fusions in insect cells and *E. coli*, respectively. For purification of the mCRY1/mPER2 complex (native and selenomethionine labeled), lysates were combined and copurified via Ni^{2+} affinity, anion exchange, and heparin and size-exclusion chromatography columns. For biochemical analysis, mCRY1 proteins were purified via Ni^{2+} affinity, anion exchange, heparin and size-exclusion columns, mPER2 proteins via Ni^{2+} affinity followed by tag cleavage, anion exchange, and size-exclusion chromatography.

Crystals of the mCRY1/mPER2 complex grew at 20°C in 0.2 M $MgCl_2$ and 12%–13% PEG3350. They contain one complex per asymmetric unit (space group $P4_32_12$).

Data Collection, Structure Determination, and Refinement

A 2.45 Å data set of a mCRY1/mPER2 crystal and a 2.8 Å data set of a selenomethione-labeled mCRY1/mPER2 crystal were collected at beamline PXII (SLS). The mCRY1/mPER2 complex structure was solved by molecular replacement with apo-mCRY1 (PDB ID 4K0R) as search model combined with selenium single-wavelength anomalous dispersion (SAD) phasing. Data collection and refinement statistics are summarized in Table S1.

Inductively Coupled Plasma Optical Emission Spectrometry

We performed inductively coupled plasma optical emission spectrometry (ICP-OES) using a Varian VISTA-RL spectrometer with a MicroMist nebulizer. Zinc binding was determined by measuring its specific emission at 213.857 nm.

Pull-Down Experiments

Clear lysates of *E. coli* cells expressing His-tagged mPER2 (WT and mutants) were incubated with Ni-Sepharose 6 Fast Flow beads in presence of 25 mM imidazole for 1 hr. After washing and equilibration in lysis buffer with 70 mM imidazole, mPER2-bound Ni-beads were incubated with clear lysates of insect cells expressing untagged mCRY1 for 1 hr in order to pull down mCRY1. The beads were extensively washed before elution of the bound complex with 500 mM imidazole and analysis by SDS-PAGE.

Native PAGE Analysis

Purified proteins were incubated at a 1:1 molar ratio in a BIS-Tris Propane buffer (pH 7.0) at 4°C for at least 2 hr. Samples were analyzed on a native 4%–20% Novex Tris-Glycine gel and by SDS-PAGE.

Circular Dichroism, Isothermal Titration Calorimetry, and Thermofluor

Circular dichroism (CD) spectroscopy using a Jasco J-810 spectropolarimeter and ITC experiments using a VP-ITC MicroCalorimeter were performed essentially as described in Czarna et al. (2011). Thermofluor was performed as described in Weir et al. (2010).

LC-ESI MS Analysis

Purified WT and mutant mCRY1/mPER2 complexes were kept under reducing (4 mM DTT) or nonreducing (no DTT, aeration) conditions for 2 days. For removal of bound zinc, the protein complex was treated with 10 mM EDTA, and zinc-bound EDTA was removed by dialysis. LC-MS analyses were performed on a Bruker micrOTOF connected to an Agilent 1100 HPLC system equipped with a diode array detector.

Luciferase Complementation Assay

The luciferase complementation assay was performed essentially as described in Kucera et al. (2012).

Analysis of Disulfide Bridges in mCRY1

mCRY1 disulfide bridges were analyzed essentially using a combined method from Wu et al. (2000) and Templeton et al. (2010). Free thiol groups in lysates of MYC-tagged mCRY1-expressing HEK293 cells were blocked with 50 mM NEM, excess NEM was removed by methanol precipitation, and disulfide bridges were then reduced with 20 mM DTT. After removal of DTT by methanol precipitation, arosen free thiol groups were modified by incubation with 300 μM Maleimide-PEG. Samples were then analyzed by western blotting using an anti-MYC antibody.

Live-Cell Zinc-Binding Assay

Human U2-OS cells stably expressing mCRY1 and mPER2 as split-luciferase hybrid proteins were kept for at least 1 week in zinc-depleted medium prior to zinc ion addition. Bioluminescence of reconstituted luciferase was recorded for several days.

^{65}Zn-Binding Assay

HEK293 cells were cultured for 5 days in zinc-free medium before transfection with equal amounts of plasmid DNA encoding either WT or mutant epitope-tagged mCRY1 or mPER2. Lysates with overexpressed V5-tagged mPER2 constructs were incubated with anti-V5 antibody and equivalent amounts of Protein G PLUS-agarose beads overnight. Beads were washed, mixed with lysates overexpressing mCRY1 or control lysates, and incubated for 3 hr with 35 μM $^{65}ZnCl_2$ radionuclide at room temperature. After washing, ^{65}Zn binding was determined by scintillation counting in a Wallac 1440 DSA system.

The Extended Experimental Procedures section, which provides detailed information about all experimental procedures, including protein purification, crystallization, structure determination, in vitro interaction studies (ITC, native gels, and pull-down), circular dichroism, thermofluor, LC-ESI-MS, and atomic absorption spectroscopy (ICP-OES), as well as cell-based studies (luciferase complementation assays, zinc-binding assays, and disulfide bond formation), is included in the Supplemental Information.

ACCESSION NUMBERS

The coordinates and structure factors have been deposited in the Protein Data Bank under the accession code 4ct0.

SUPPLEMENTAL INFORMATION

Supplemental Information includes Extended Experimental Procedures, seven figures, and two tables and can be found with this article online at http://dx.doi.org/10.1016/j.cell.2014.03.057.

AUTHOR CONTRIBUTIONS

I.S., S.R., T.W., R.K., A.K., and E.W. designed experiments; I.S., S.R., T.W., R.K., C.B., and A.G. performed experiments; I.S., J.R.P., and C.B. solved the structure; I.S., S.R., T.W., R.K., J.R.P., C.B., A.K., and E.W. analyzed data; and I.S., A.K., and E.W. wrote the paper.

ACKNOWLEDGMENTS

We thank the beamline staff at Swiss Light Source (SLS, Villingen) for excellent assistance and the Max Planck Institute (MPI) of Biochemistry Crystallization Facility and Biochemistry Core Facility, especially Elisabeth Wehyer-Stingl, for technical assistance and support. Further, we thank Helmut Hartl and Jaroslava Obel (Department of Chemistry and Pharmacy, LMU Munich) for ICP-OES analysis. We thank our colleagues of the Department of Structural Cell Biology at the MPI of Biochemistry for help with data collection, fruitful discussions, and critical comments. We are indebted to Claire Basquin for assistance with ITC, thermofluor, and other biophysical methods and to Michaela Rode for assistance with insect cell culture. Anna Czarna, Sebastian Falk, Kai Hell, Debora Makino, Michael Taschner, and Justine Witosch are thanked for valuable suggestions and discussions. This study was supported by DFG grants Wo695-3 (FOR526), Wo695-4, and Wo695-6 to E.W., DFG grant SFB740/D2 to A.K., and a fellowship of the Studienstiftung des deutschen Volkes to I.S.

Received: September 4, 2013
Revised: February 6, 2014
Accepted: March 17, 2014
Published: May 22, 2014

REFERENCES

Auld, D.S. (2001). Zinc coordination sphere in biochemical zinc sites. Biometals *14*, 271–313.

Barclay, J.L., Shostak, A., Leliavski, A., Tsang, A.H., Jöhren, O., Müller-Fielitz, H., Landgraf, D., Naujokat, N., van der Horst, G.T.J., and Oster, H. (2013). High-fat diet-induced hyperinsulinemia and tissue-specific insulin resistance in Cry-deficient mice. Am. J. Physiol. Endocrinol. Metab. *304*, E1053–E1063.

Chaves, I., Yagita, K., Barnhoorn, S., Okamura, H., van der Horst, G.T.J., and Tamanini, F. (2006). Functional evolution of the photolyase/cryptochrome protein family: importance of the C terminus of mammalian CRY1 for circadian core oscillator performance. Mol. Cell. Biol. *26*, 1743–1753.

Czarna, A., Breitkreuz, H., Mahrenholz, C.C., Arens, J., Strauss, H.M., and Wolf, E. (2011). Quantitative analyses of cryptochrome-mBMAL1 interactions: mechanistic insights into the transcriptional regulation of the mammalian circadian clock. J. Biol. Chem. *286*, 22414–22425.

Czarna, A., Berndt, A., Singh, H.R., Grudziecki, A., Ladurner, A.G., Timinszky, G., Kramer, A., and Wolf, E. (2013). Structures of Drosophila cryptochrome and mouse cryptochrome1 provide insight into circadian function. Cell *153*, 1394–1405.

Eckel-Mahan, K., and Sassone-Corsi, P. (2009). Metabolism control by the circadian clock and vice versa. Nat. Struct. Mol. Biol. *16*, 462–467.

Edgar, R.S., Green, E.W., Zhao, Y., van Ooijen, G., Olmedo, M., Qin, X., Xu, Y., Pan, M., Valekunja, U.K., Feeney, K.A., et al. (2012). Peroxiredoxins are conserved markers of circadian rhythms. Nature *485*, 459–464.

Eide, E.J., Vielhaber, E.L., Hinz, W.A., and Virshup, D.M. (2002). The circadian regulatory proteins BMAL1 and cryptochromes are substrates of casein kinase Iepsilon. J. Biol. Chem. *277*, 17248–17254.

Evans, J.C., Huddler, D.P., Jiracek, J., Castro, C., Millian, N.S., Garrow, T.A., and Ludwig, M.L. (2002). Betaine-homocysteine methyltransferase: zinc in a distorted barrel. Structure *10*, 1159–1171.

Gatfield, D., and Schibler, U. (2007). Physiology. Proteasomes keep the circadian clock ticking. Science *316*, 1135–1136.

Griffin, E.A., Jr., Staknis, D., and Weitz, C.J. (1999). Light-independent role of CRY1 and CRY2 in the mammalian circadian clock. Science *286*, 768–771.

Hirano, A., Yumimoto, K., Tsunematsu, R., Matsumoto, M., Oyama, M., Kozuka-Hata, H., Nakagawa, T., Lanjakornsiripan, D., Nakayama, K.I., and Fukada, Y. (2013). FBXL21 regulates oscillation of the circadian clock through ubiquitination and stabilization of cryptochromes. Cell *152*, 1106–1118.

Hirota, T., Lee, J.W., St John, P.C., Sawa, M., Iwaisako, K., Noguchi, T., Pongsawakul, P.Y., Sonntag, T., Welsh, D.K., Brenner, D.A., et al. (2012). Identification of small molecule activators of cryptochrome. Science *337*, 1094–1097.

Hitomi, K., DiTacchio, L., Arvai, A.S., Yamamoto, J., Kim, S.-T., Todo, T., Tainer, J.A., Iwai, S., Panda, S., and Getzoff, E.D. (2009). Functional motifs in the (6-4) photolyase crystal structure make a comparative framework for DNA repair photolyases and clock cryptochromes. Proc. Natl. Acad. Sci. USA *106*, 6962–6967.

Huang, N., Chelliah, Y., Shan, Y., Taylor, C.A., Yoo, S.-H., Partch, C., Green, C.B., Zhang, H., and Takahashi, J.S. (2012). Crystal structure of the heterodimeric CLOCK:BMAL1 transcriptional activator complex. Science *337*, 189–194.

Ilbert, M., Graf, P.C., and Jakob, U. (2006). Zinc center as redox switch—new function for an old motif. Antioxid. Redox Signal. *8*, 835–846.

King, D.P., Vitaterna, M.H., Chang, A.M., Dove, W.F., Pinto, L.H., Turek, F.W., and Takahashi, J.S. (1997). The mouse Clock mutation behaves as an antimorph and maps within the W19H deletion, distal of Kit. Genetics *146*, 1049–1060.

Koike, N., Yoo, S.-H., Huang, H.-C., Kumar, V., Lee, C., Kim, T.-K., and Takahashi, J.S. (2012). Transcriptional architecture and chromatin landscape of the core circadian clock in mammals. Science *338*, 349–354.

Kucera, N., Schmalen, I., Hennig, S., Öllinger, R., Strauss, H.M., Grudziecki, A., Wieczorek, C., Kramer, A., and Wolf, E. (2012). Unwinding the differences of the mammalian PERIOD clock proteins from crystal structure to cellular function. Proc. Natl. Acad. Sci. USA *109*, 3311–3316.

Kume, K., Zylka, M.J., Sriram, S., Shearman, L.P., Weaver, D.R., Jin, X., Maywood, E.S., Hastings, M.H., and Reppert, S.M. (1999). mCRY1 and mCRY2 are essential components of the negative limb of the circadian clock feedback loop. Cell *98*, 193–205.

Lamia, K.A., Sachdeva, U.M., DiTacchio, L., Williams, E.C., Alvarez, J.G., Egan, D.F., Vasquez, D.S., Juguilon, H., Panda, S., Shaw, R.J., et al. (2009). AMPK regulates the circadian clock by cryptochrome phosphorylation and degradation. Science *326*, 437–440.

Lamia, K.A., Papp, S.J., Yu, R.T., Barish, G.D., Uhlenhaut, N.H., Jonker, J.W., Downes, M., and Evans, R.M. (2011). Cryptochromes mediate rhythmic repression of the glucocorticoid receptor. Nature *480*, 552–556.

Marcheva, B., Ramsey, K.M., Buhr, E.D., Kobayashi, Y., Su, H., Ko, C.H., Ivanova, G., Omura, C., Mo, S., Vitaterna, M.H., et al. (2010). Disruption of the clock components CLOCK and BMAL1 leads to hypoinsulinaemia and diabetes. Nature *466*, 627–631.

Maret, W. (2012). New perspectives of zinc coordination environments in proteins. J. Inorg. Biochem. *111*, 110–116.

Miyazaki, K., Mesaki, M., and Ishida, N. (2001). Nuclear entry mechanism of rat PER2 (rPER2): role of rPER2 in nuclear localization of CRY protein. Mol. Cell. Biol. *21*, 6651–6659.

Müller, M., and Carell, T. (2009). Structural biology of DNA photolyases and cryptochromes. Curr. Opin. Struct. Biol. *19*, 277–285.

O'Neill, J.S., and Reddy, A.B. (2011). Circadian clocks in human red blood cells. Nature *469*, 498–503.

O'Neill, J.S., van Ooijen, G., Dixon, L.E., Troein, C., Corellou, F., Bouget, F.-Y., Reddy, A.B., and Millar, A.J. (2011). Circadian rhythms persist without transcription in a eukaryote. Nature *469*, 554–558.

Okano, S., Akashi, M., Hayasaka, K., and Nakajima, O. (2009). Unusual circadian locomotor activity and pathophysiology in mutant CRY1 transgenic mice. Neurosci. Lett. *451*, 246–251.

Okano, S., Hayasaka, K., Igarashi, M., Iwai, H., Togashi, Y., and Nakajima, O. (2010). Non-obese early onset diabetes mellitus in mutant cryptochrome1 transgenic mice. Eur. J. Clin. Invest. *40*, 1011–1017.

Okano, S., Hayasaka, K., Igarashi, M., Togashi, Y., and Nakajima, O. (2013). Characterization of age-associated alterations of islet function and structure in diabetic mutant cryptochrome 1 transgenic mice. J. Diabetes Investigation *4*, 428–435.

Oteiza, P.I. (2012). Zinc and the modulation of redox homeostasis. Free Radic. Biol. Med. *53*, 1748–1759.

Ozber, N., Baris, I., Tatlici, G., Gur, I., Kilinc, S., Unal, E.B., and Kavakli, I.H. (2010). Identification of two amino acids in the C-terminal domain of mouse CRY2 essential for PER2 interaction. BMC Mol. Biol. *11*, 69.

Templeton, D.J., Aye, M.-S., Rady, J., Xu, F., and Cross, J.V. (2010). Purification of reversibly oxidized proteins (PROP) reveals a redox switch controlling p38 MAP kinase activity. PLoS ONE *5*, e15012.

Tomita, T., Miyazaki, K., Onishi, Y., Honda, S., Ishida, N., and Oishi, K. (2010). Conserved amino acid residues in C-terminus of PERIOD 2 are involved in interaction with CRYPTOCHROME 1. Biochim. Biophys. Acta *1803*, 492–498.

van der Horst, G.T., Muijtjens, M., Kobayashi, K., Takano, R., Kanno, S., Takao, M., de Wit, J., Verkerk, A., Eker, A.P., van Leenen, D., et al. (1999). Mammalian Cry1 and Cry2 are essential for maintenance of circadian rhythms. Nature *398*, 627–630.

Wang, T.A., Yu, Y.V., Govindaiah, G., Ye, X., Artinian, L., Coleman, T.P., Sweedler, J.V., Cox, C.L., and Gillette, M.U. (2012). Circadian rhythm of redox state regulates excitability in suprachiasmatic nucleus neurons. Science *337*, 839–842.

Weir, J.R., Bonneau, F., Hentschel, J., and Conti, E. (2010). Structural analysis reveals the characteristic features of Mtr4, a DExH helicase involved in nuclear RNA processing and surveillance. Proc. Natl. Acad. Sci. USA *107*, 12139–12144.

Wu, H.H., Thomas, J.A., and Momand, J. (2000). p53 protein oxidation in cultured cells in response to pyrrolidine dithiocarbamate: a novel method for relating the amount of p53 oxidation in vivo to the regulation of p53-responsive genes. Biochem. J. *351*, 87–93.

Xing, W., Busino, L., Hinds, T.R., Marionni, S.T., Saifee, N.H., Bush, M.F., Pagano, M., and Zheng, N. (2013). SCF(FBXL3) ubiquitin ligase targets cryptochromes at their cofactor pocket. Nature *496*, 64–68.

Yagita, K., Tamanini, F., Yasuda, M., Hoeijmakers, J.H.J., van der Horst, G.T.J., and Okamura, H. (2002). Nucleocytoplasmic shuttling and mCRY-dependent inhibition of ubiquitylation of the mPER2 clock protein. EMBO J. *21*, 1301–1314.

Ye, R., Selby, C.P., Ozturk, N., Annayev, Y., and Sancar, A. (2011). Biochemical analysis of the canonical model for the mammalian circadian clock. J. Biol. Chem. *286*, 25891–25902.

Yoo, S.-H., Mohawk, J.A., Siepka, S.M., Shan, Y., Huh, S.K., Hong, H.-K., Kornblum, I., Kumar, V., Koike, N., Xu, M., et al. (2013). Competing E3 ubiquitin ligases govern circadian periodicity by degradation of CRY in nucleus and cytoplasm. Cell *152*, 1091–1105.

Young, M.W., and Kay, S.A. (2001). Time zones: a comparative genetics of circadian clocks. Nat. Rev. Genet. *2*, 702–715.

Zhang, E.E., Liu, Y., Dentin, R., Pongsawakul, P.Y., Liu, A.C., Hirota, T., Nusinow, D.A., Sun, X., Landais, S., Kodama, Y., et al. (2010). Cryptochrome mediates circadian regulation of cAMP signaling and hepatic gluconeogenesis. Nat. Med. *16*, 1152–1156.